Materials Transactions, Vol. 46, No. 7 (2005) pp. 1618 to 1626
Special Issue on Medical, Healthcare, Sport and Leisure Materials

Biocompatibility Evaluation of Ti–15Al–33Nb(at%) and Ti–21Al–29Nb(at%)

Carl J. Boehlert[1], Katherine A. Rider[2] and Lisa M. Flick[2]

[1]*Department of Chemical Engineering and Materials Science, Michigan State University, East Lansing, Michigan, 48824, U.S.A.*
[2]*Biology Department, Alfred University, Alfred, New York, 14802, U.S.A.*

In this work the biocompatibility of two vanadium-free Ti–Al–Nb alloys, Ti–15Al–33Nb and Ti–21Al–29Nb, was evaluated and compared to that for commercially pure titanium (CP Ti) and alumina (Al_2O_3). Fine particles were milled from sheet-processed material and implanted onto mice calvaria using an established animal model. Various stains, including methylene blue/acid fuchsin, TRAcP, and immunohistochemistry, were used on the particle-treated calvaria to measure the extent of bone deterioration of the calvaria, quantify the amount of osteoclasts, and approximate the presence of T-cells. In addition, reaction with particle-stimulated macrophages was observed and the production of the cytokine TNFα was recorded and quantified. The results indicated that the Ti–Al–Nb alloys statistically outperformed both CP Ti and Al_2O_3 in terms of their overall biocompatibility with respect to the experiments performed.

(Received January 28, 2005; Accepted April 20, 2005; Published July 15, 2005)

Keywords: *titanium-aluminum-niobium alloy, biocompatibility, stains, T-cells, osteoclasts, particles*

1. Introduction

Currently, more than 1.3 million joint replacement surgeries are performed each year worldwide,[1)] and this number is expected to increase considering the increasing age of the population. When an implant fails, revision arthroplasty is required, which has a poorer clinical result and shorter duration of survival than the primary joint replacement.[2)] Implant failure frequently occurs as a result of osteolysis which is defined as a decrease in bone volume and is characterized by a two millimeter gap between prosthesis and bone as seen in radiographs from arthroplasty patients. Osteolysis can be explained by wear debris generated from the prosthesis which is phagocytosed by macrophages (at the bone-implant interface), which produce proinflamatory cytokines such as tumor necrosis factor α (TNFα), interleukin-1 (IL-1), and IL-6.[3–9)] Release of these cytokines leads to an inflammatory response characterized by the activation and recruitment of osteoclasts, which resorb bone after differentiation and activation, to the bone/implant interface and the formation of a periprosthetic membrane.[10–12)] Due to several factors discussed elsewhere,[13–18)] TNFα is considered to be one of the critical cytokines involved in wear debris-induced osteolysis. Using an animal model of particle-induced osteolysis in which polymethylmethacrylate (PMMA) or CP Ti particles were implanted onto mouse calvaria,[19,20)] TNFα signaling has been demonstrated to be critical to the development of the inflammatory osteolytic response to wear debris. Overall, up to 20% of patients with total joint replacement will demonstrate evidence of osteolysis within ten years where wear debris-induced osteolysis is the leading culprit, and this currently does not have a proven drug therapy.[21–23)] Thus prevention of osteolysis and prosthetic implant loosening is clearly desirable, and one means to address this issue is through evaluation and improvement of biomedical implant materials and their interaction with living cell and bone tissue.

Due to their exceptional biocompatibility characteristics, CP Ti and α/β type Ti alloys are currently widely used as structural biomaterials for the replacement of hard tissues in devices such as artificial hip joints and dental implants. In particular, Ti–6Al–4V(wt%) is widely used because of its excellent biocompatibility and its combination of high specific strength, fracture toughness, fatigue and corrosion resistance, ductility, low density, elastic modulus, and conventional processability. However, V is potentially toxic in elemental form;[24)] therefore, other alloying elements are currently being examined. In fact, new Ti alloys, targeted for biomedical applications and void of V, are now being included in American Society for Testing and Materials standards.[25,26)] The recent trend in research and development of Ti alloys for biomedical applications is to develop low rigidity β-type alloys composed of non-toxic and non-allergic elements with attractive mechanical properties.[27)] In this regard, several authors have been evaluating alloys based on the Ti–Al–Nb system, such as Ti–6Al–7Nb(wt%) [Ti–10.5Al–3.6Nb(at%)].[28–36)] Recently Boehlert *et al.*[37)] have shown that Ti–15Al–33Nb(at%) and Ti–21Al–29Nb(at%)[38)] exhibit attractive mechanical properties for biomedical applications where the ambient-temperature tensile and fatigue strengths compared favorably to those for Ti–6Al–4V(wt%), while their modulus was slightly lower than that for Ti–6Al–4V(wt%). The current work is an extension of that previous work where the biocompatibility of particles taken from these two Ti–Al–Nb alloys were evaluated and their behavior with respect to interaction with living cells and bone tissue was directly compared to that for CP Ti and Al_2O_3.

2. Experimental Procedures

2.1 Material Processing

The details of the Ti–Al–Nb alloy processing have been described previously.[37)] Briefly, the alloys were cast into 15 cm diameter ingots, which were then multistep forged to approximately 14 cm by 7 cm by 58 cm. Approximately 1.6 cm thick slabs were then cut from the transverse sections of the ingots and hot rolled to 1.65 mm thick by 7 cm wide sheets. The hot rolling produced a reduction in area of 90%

and introduced a total effective true shear strain on the order of two. Identical hot-working temperatures, which were always maintained below the BCC-phase transus temperature, were used for the forging and rolling operations for a given alloy. The Ti–15Al–33Nb sheets were hot rolled at 899°C and the Ti–21Al–29Nb sheets were hot rolled at 982°C. After the hot rolling was complete, the sheets were annealed at their respective rolling temperatures for one hour and then air-cooled. All alloy processing was performed by RMI Titanium, Company (Niles, Ohio, U.S.A.). The chemical compositions of the rolled sheets were determined using Inductively Coupled Plasma Optical Emission Spectroscopy (ICP-OES) and Inert Gas Fluorescence (IGF). The Ti–Al–Nb alloy particles used for the experiments were first filed from the sheet samples. Approximately five grams of the filings were then shipped out to Spex CertiPrep, Inc. (Metuchen, NJ, U.S.A.) for further breakdown. The softer and ductile Ti–15Al–33Nb filings were milled for 20 minutes using Shatterbox 8515 and a Zirconia Grinding Container 8506 along with 10 ml of Vertrel XF, a fluorocarbon fluid which prevents particles from welding together under pressure, as a grinding aid. The harder and brittle Ti–21Al–29Nb filings were broken down for two hours in a 8004 Tungsten Carbide Vial, 8000M Mixer/Mill using 6 ml of Vertrel XF. The size distribution of the resulting particles was measured using both scanning electron microscopy (SEM) coupled with image analysis and a light scattering technique for powder suspensions.[39,40] The SEM used was an AMRAY 1810 SEM and the light-scattering device was a Leeds Northrup Instruments Microtrac FRA. The results from these analysis indicated that the Ti–15Al–33Nb particles ranged in size from 2–60 μm and the average particle diameter was 13.6 μm, see Fig. 1(a). The Ti–21Al–29Nb particles ranged in size from 1–20 μm and the average particle diameter was 6.1 μm, see Fig. 1(b). CP Ti particles, obtained from Johnson Mathey Chemicals (Ward Hill, MA, U.S.A.), were also evaluated, and the particle preparation was described previously.[41,42] SEM measurements indicated that 90% of these particles were less than 10 μm in diameter. Alumina oxide powers were purchased from Alfa Aesar (Ward Hill, MA, U.S.A.) and the SEM measurements indicated that they ranged between 0.5–5 μm in diameter.

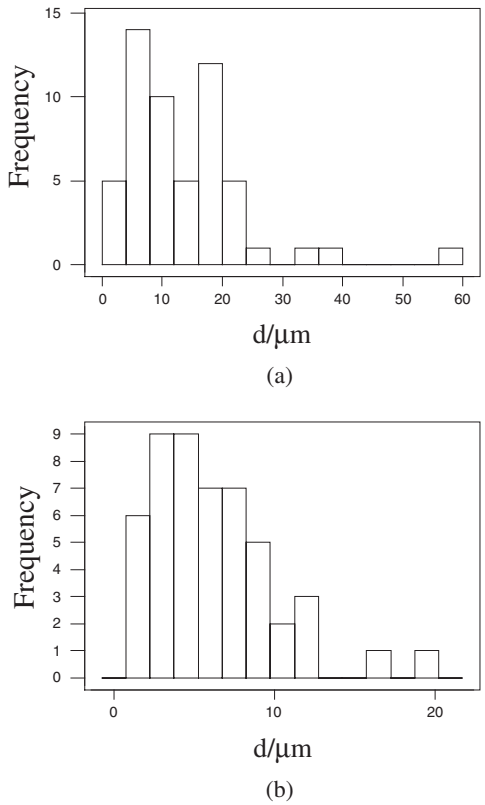

Fig. 1 Representative particle size distribution for (a) Ti–15Al–33Nb and (b) Ti–21Al–29Nb.

2.2 Particle Implantation

A mouse calvaria model of wear debris-induced bone loss, including quantification of in vivo osteoclast numbers, was utilized where implantation of particles in the mice was performed following the procedure discussed previously.[41–43] Briefly, five or six healthy homozygous C57BL/6 mice (The Jackson Laboratory, Bar Harbor, ME) were used in each group. All animals were housed and treated according to guidelines approved by the Alfred University Institutional Animal Care and Use Committee. Mice were anesthetized with 70–80 mg/kg of ketamine and 5–7 mg/kg of xylazine by intraperitoneal (i.p.) injection. A $1 \times 1\,cm^2$ area of calvarial bone was exposed by making a midline sagittal incision over the calvaria, leaving the periosteum intact. Approximately 30 mg of the particles were spread over the area and the incision was closed. Baseline animals did not undergo surgery nor received particle implantation. Ten days after surgery the mice were sacrificed and the calvaria were harvested. Each calvarium was cut in half laterally such that the midline suture was in the center of the cross-section. They were then fixed in 10% buffered neutral formalin (Pharmco Products Inc., Brookfield, CT, U.S.A.) for 24 hours. The calvaria were next decalcified in 10%EDTA (pH = 7.2) for one week. The calvaria were then processed, embedded in paraffin, and cut into 5 μm sections using a Microm 310 microtome (Richard-Allan Scientific, Kalamazoo, MI, U.S.A.). These sections were then placed onto slides and let sit overnight at 75°C in an oven. After baking overnight, the slides were deparaffinized for four minutes in four separate xylenes and rehydrated in a series of ethanol solutions prior to performing the staining procedures.

2.3 Methylene Blue/Acid Fuchsin Staining

The amount of bone deterioration was quantified using a new differential stain for bone and soft tissue.[44] Briefly, slides were deparaffinized and rehydrated, set in 0.2% methylene blue (Fisher Scientific, Fairlawn, NJ, U.S.A.) for 30 seconds, rinsed and incubated in acid fuchsin (Fisher Scientific) for five minutes. The stained slides were then dehydrated, cleared, and coverslipped then observed using an Olympus IX51 (Melville, NY, U.S.A.) inverted optical microscope (OM) at 40× magnification. Using Scion Image (Scion Corp., Frederick, MD, U.S.A.) software, the area of soft tissue between the parietal bones of the midline sagittal suture was traced and measured. These measurements of the particle-treated calvaria were compared with the measurements from calvaria that were not treated.

2.4 TRAcP Staining

Osteoclasts are multinucleated cells which are derived from monocyte precursors and resorb bone. Therefore, the more osteoclasts present, the more deterioration of the calvaria bone. The number of TRAcP+ osteoclasts was determined in calvarial sections using a cytochemical staining technique. Positive control slides of mouse tibia were also stained. Slides were incubated in a naphthol AS-BI phosphate (Sigma) substrate solution at 37°C for 45 minutes followed by treatment in pararosaniline-nitrite dye for 6 minutes. Slides were then counterstained with hematoxylin. Each section was digitally photographed at 40× magnification using the OM and the number of TRAcP+ cells within the midline sagittal suture area was counted.

2.5 Immunohistochemistry Staining

The immunohistochemistry stain highlights the T-cells present in the particle-treated calvaria as a result of chemokine-mediated T-cell migration to the calvaria. Immunohistochemistry was performed on calvaria and spleen (positive control) sections following citrate buffer antigen retrieval using an antibody to the pan-T-cell marker CD3ε (Santa Cruz Biotechnology, Santa Cruz, CA, U.S.A.). VECTASTAIN ABC and NovaRED substrate kits (Vector Laboratories, Burlingame, CA, U.S.A.) were used to develop the sections which were then counterstained with hematoxylin. The slides were observed using the OM at 40× magnification, and photographed using the Olympus DP12 digital camera (Melville, NY, U.S.A.).

2.6 Cytokine Production in vitro

RAW 264.7 murine macrophage cell line was obtained from the American Type Culture Collection (Rockville, MD, U.S.A.) and grown in Dulbecco's Modified Eagle's Medium (DMEM; Sigma) supplemented with 10% fetal bovine serum and 1% antibiotic/antimycotic solution (Gibco, Grand Island, NY, U.S.A.). 8×10^5 cells were plated into each well of a 6-well culture plate and stimulated with various concentrations of CP Ti, Al_2O_3, Ti–15Al–33Nb and Ti–21Al–29Nb for 24 hours. Cells were photographed using the OM at 100× magnification and culture media was collected for analysis. TNFα was determined by enzyme-linked immunosorbent assay (ELISA) using antibodies and recombinant standards obtained from R&D Systems (Minneapolis, MN, U.S.A.) as previously described.[42] The recombinant standard was used to create a standard curve from which the concentration of TNFα in the samples could be calculated.

2.7 Statistical Analysis

Statistical significance was determined using Student's t-test where values less than $p = 0.05$ were considered significant for single comparisons.

2.8 Electron Microscopy Characterization

2.8.1 Microstructure

Characterization of the as-processed Ti–Al–Nb sheet microstructures was carried out using OM, SEM, and X-ray diffraction (XRD) analysis. Sheet samples were diamond cut and mounted in epoxy then ground using successively finer grits of silicon carbide paper. After grinding, the samples were polished using diamond paste according to the following schedule: 30 µm for five minutes, 15 µm for five minutes, 6 µm for five minutes, 1 µm for 20 minutes. Colloidal silica with an average particle size of 0.06 µm was used for the final polish. SEM images were obtained using an AMRAY 1810 SEM. The constituted phases were examined through XRD analysis, carried out using a Cu target with an accelerating voltage of 40 kV and a current of 30 mA.

2.8.2 Particle-Treated Calvaria

Extracted calvaria were placed in 1×PBS for approximately five hours. The samples were then transferred to 70% ethanol for two days then placed in a weighing tray to dry at

Table 1 Ti–Al–Nb Alloy compositions.

Alloy	Ti (at%)	Al (at%)	Nb (at%)	Fe (ppm)	O (ppm)	N (ppm)
Ti–15Al–33Nb	51.4	15.3	33.3	110	1100	100
Ti–21Al–29Nb	50.7	20.6	28.7	2000	790	110

ppm: parts per million

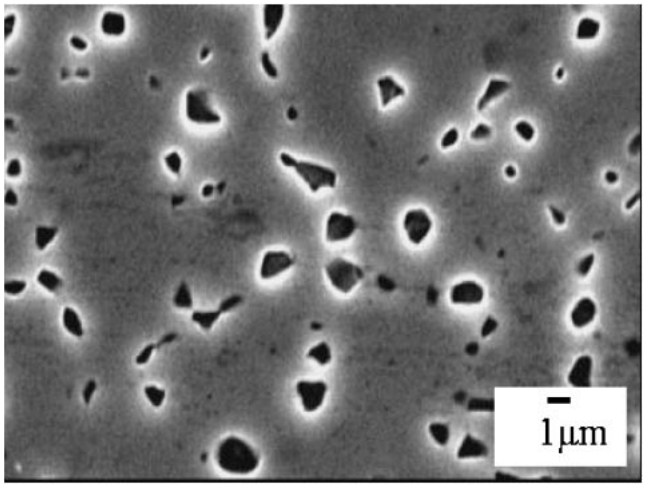

(a)

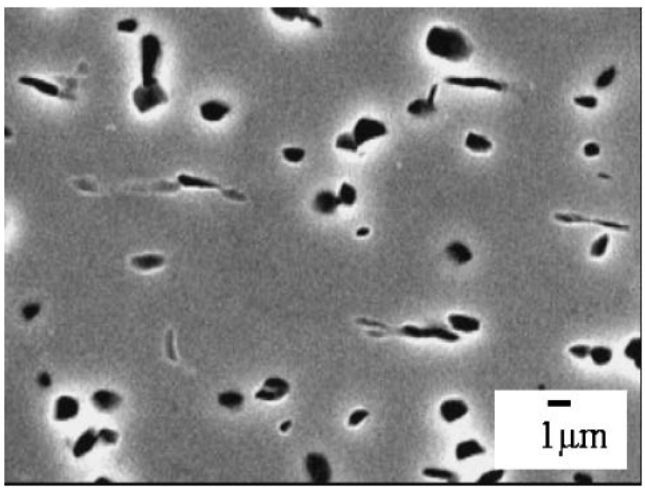

(b)

Fig. 2 SEM images of the as-processed (a) Ti–15Al–33Nb and (a) Ti–21Al–29Nb sheet microstructures. The matrix consists of the body-centered cubic phase and the dark phase is hexagonal close packed.

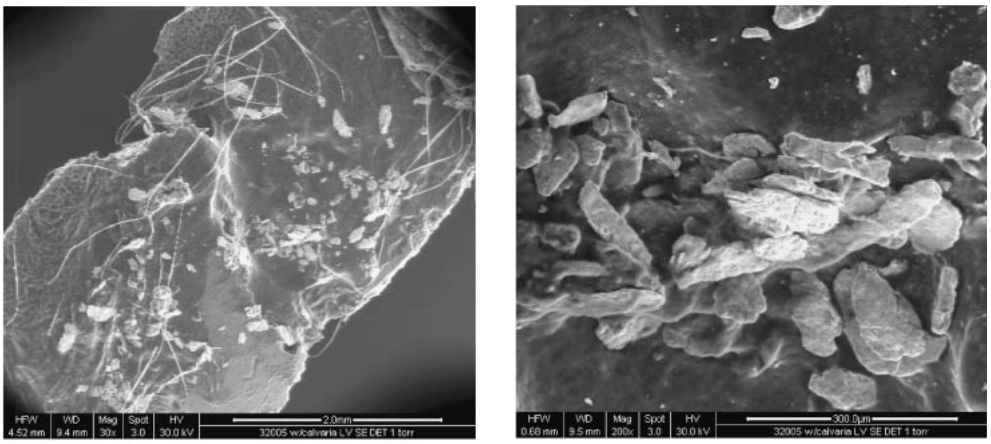

(a) (b)

Fig. 3 (a) Low- and (a) high-magnification ESEM images of Ti–15Al–33Nb particle-treated calvaria indicating a coherently-bonded interface. These images indicate that the particles (lighter) were denser than the calvaria soft and hard tissue (darker). No adverse reactions were noted with the cantilever or the soft tissue for 10 days after attachment of the particles.

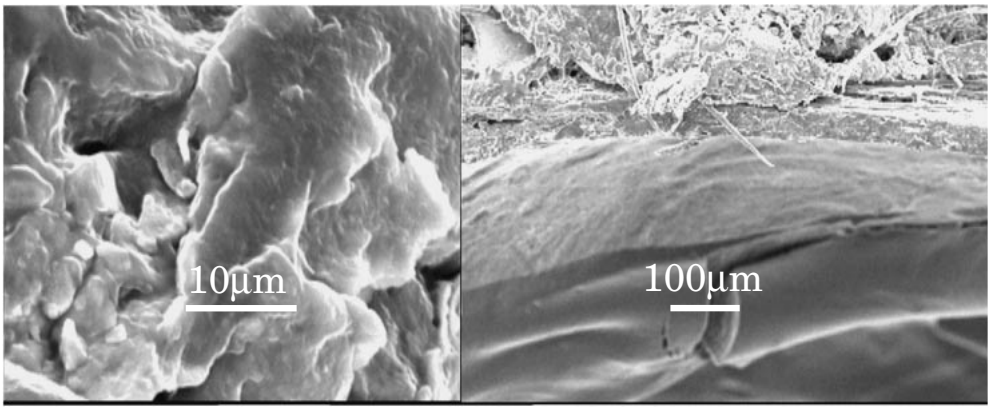

(a) (b)

Fig. 4 (a) Low- and (b) high-Magnification SEM images of the interface between Ti–21Al–29Nb powders and a mouse calvaria indicating the coherent interface. No adverse reactions were noted with the cantilever or the soft tissue.

room temperature. OM images of the calvaria samples were then obtained. Samples were then secured to SEM stubs using colloidal graphite and vacuum sputter-coated with a thin gold-palladium layer order to ensure conductivity of the samples for SEM imaging, performed using a Phillips model 515 SEM. Multiple SEM magnifications were used to examine the boundary between bone and particles on the samples. Energy dispersive spectroscopy (EDS) analysis was performed on the calvaria, particles, and the interface between the calvaria and particles. The particle interaction with the calvaria was also characterized using a Quanta 200 environmental scanning microscope (ESEM) in low-vacuum mode where no conductive coating was necessary.

3. Results and Discussion

3.1 Microstructure

The measured chemical compositions of the Ti–Al–Nb alloys are provided in Table 1 and the as-processed sheet microstructures are shown in Figs. 2(a) and (b). The as-processed alloys were composed almost entirely ($\geq$90% by volume[37]) of the body-centered-cubic phase and smaller quantities of the orthorhombic and hexagonal-close-packed phase were dispersed throughout the sample.

3.2 Imaging of Treated Calvaria

OM, SEM, and EDS analysis confirmed that no significant detrimental reaction occurred between the Ti–Al–Nb alloy particles and the calvaria. Figs. 3(a) and (b) illustrate ESEM images of the interaction between the Ti–15Al–33Nb particles and the calvaria. The particles appeared to have adhered well with the calvaria where no interfacial cracking or detrimental reaction layer were observed, see Figs. 4(a) and (b). The EDS spectra taken from the calvaria region indicated carbon, oxygen, phosphorous, and calcium were present while analysis of the particles indicated Al, Nb, and Ti were present. For EDS analysis of the boundary between the particles and calvaria, elements from both components were observed further indicating that there was some interaction between the calvaria and particles.

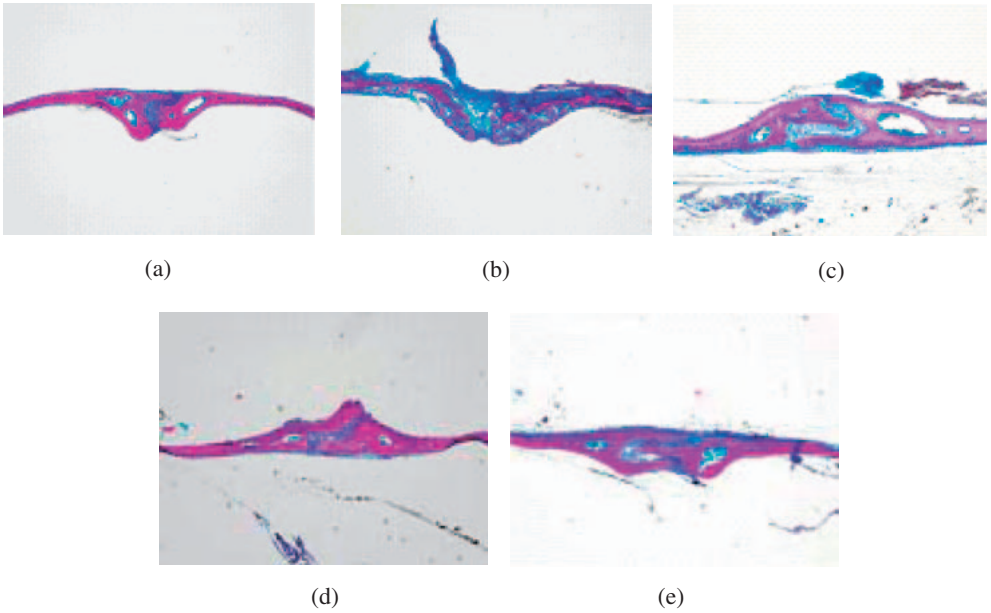

Fig. 5 OM images (40×) of methylene blue/acid fuchsin-stained (a) baseline and non-particle treated calvaria and (b) Al_2O_3-, (c) CP Ti-, (d) Ti–15Al–33Nb-, and (e) Ti–21Al–29Nb-treated calvaria. Pink staining indicates bone tissue. Note the wider midline sagittal suture (blue staining) in panels b and c.

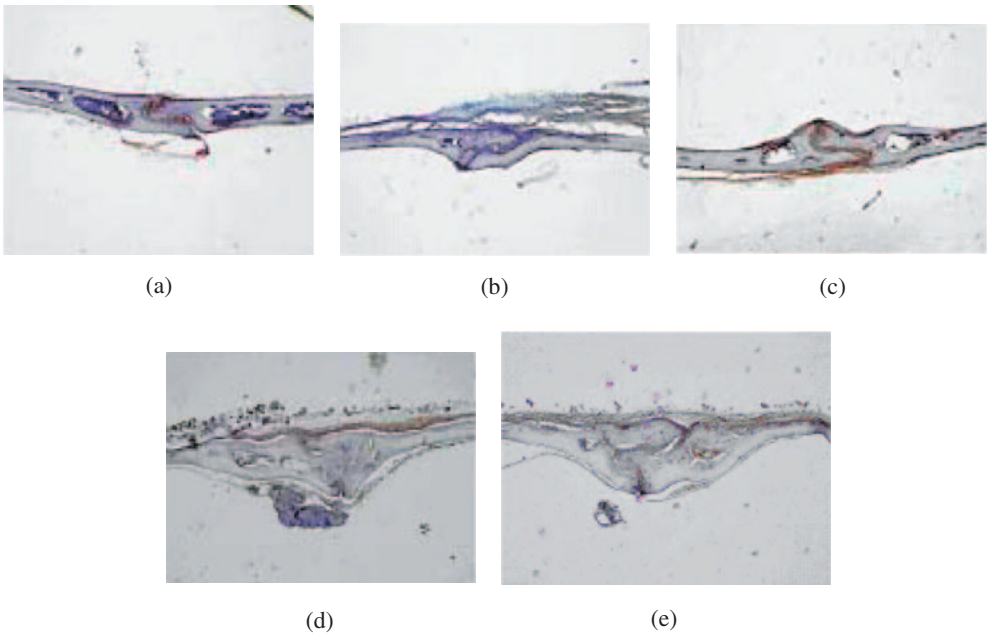

Fig. 7 OM images (40×) of immunohistochemistry-stained (a) baseline and non-particle treated calvaria and (b) Al_2O_3-, (c) CP Ti-, (d) Ti–15Al–33Nb-, and (e) Ti–21Al–29Nb-treated calvaria. Reddish-brown staining indicates the presence of T-cells in the section.

3.3 Methylene Blue/Acid Fuchsin

The amount of bone deterioration was quantified by using a methylene blue/acid fuchsin stain imaged optically at 40× magnification, see Fig. 5. As compared to the baseline samples, the bone edges for the particle-treated samples were more jagged indicating that there was more deterioration that took place in the particle-treated samples. The Scion Image software was used to trace the center portion of the calvaria. Once traced, the program computes the total area enclosed, and this is the total midline sagittal suture area (MSA). The difference between the average MSA for the baseline and treated samples represents the amount of bone deterioration in response to the particles. In comparing the particle-treated samples, Ti–15Al–33Nb- and Ti–21Al–29Nb-treated samples showed the least amount of deterioration, see Table 2, where the Ti–21Al–29Nb-treated samples exhibited slightly more deterioration than Ti–15Al–33Nb. In comparing the Al_2O_3, and CP Ti-treated particles, it was found that slightly more deterioration occurred in the Al_2O_3-treated samples. The overall measurement for the baseline was found to be

Table 2 Area measurements (in mm^2) of the relative bone deterioration for the particle-treated calvaria samples.

Baseline 1	0.0728	Average
Baseline 2	0.1338	
Baseline 3	0.0551	0.1383
Baseline 4	0.2353	
Baseline 5	0.2027	
Baseline 6	0.1298	
Al_2O_3 1	0.2814	
Al_2O_3 2	0.3255	
Al_2O_3 3	0.4207	0.3272
Al_2O_3 4	0.1325	
Al_2O_3 5	0.2895	
Al_2O_3 6	0.5134	
CP Ti 1	0.3786	
CP Ti 2	0.2404	
CP Ti 3	0.2272	0.2959
CP Ti 4	0.3762	
CP Ti 5	0.2572	
Ti–15Al–33Nb 1	0.1246	
Ti–15Al–33Nb 2	0.1287	
Ti–15Al–33Nb 3	0.2455	0.1497
Ti–15Al–33Nb 4	0.1715	
Ti–15Al–33Nb 5	0.0782	
Ti–21Al–29Nb 1	0.1975	
Ti–21Al–29Nb 2	0.1406	
Ti–21Al–29Nb 3	0.3069	0.1862
Ti–21Al–29Nb 4	0.1426	
Ti–21Al–29Nb 5	0.1433	

$0.1382\,mm^2$ followed by Ti–15Al–33Nb and Ti–21Al–29Nb-treated samples with measurements of 0.1497 and $0.1862\,mm^2$ respectfully, which were significantly lower than those for the Al_2O_3-treated ($0.3272\,mm^2$) and CP Ti-treated ($0.2959\,mm^2$) samples. The difference between the measurements for the Al_2O_3- and CP Ti-treated samples was not statistically significant.

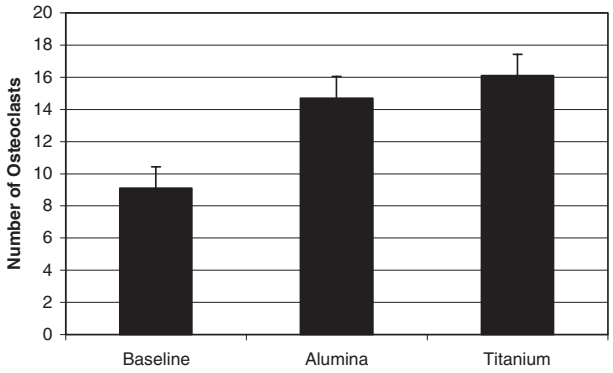

Fig. 6 Bar chart indicating the average number of osteoclasts observed in the particle-treated calvaria.

3.4 TRAcP

The number of osteoclasts present in both non-treated and particle-treated samples was measured using the TRAcP stain. Osteoclasts were counted using the OM at 40× for the baseline, Al_2O_3- and CP Ti-treated calvaria samples. It was found that the CP Ti-treated samples contained the most osteoclasts while the baseline samples contained the least amount. The baseline, Al_2O_3-, and CP Ti-treated samples contained an average of 9.1, 14.7, and 16.1 osteoclasts, respectively (see Table 3 and Fig. 6). Statistical analysis indicated that the baseline value was statistically significant compared to that for both the Al_2O_3- ($p = 0.0001$) and CP Ti-treated samples, however the difference between the

Table 3 Amount of osteoclasts present in baseline, Al_2O_3- and CP Ti-treated calvaria samples.

Sample	Sets 1–3	Ave.	Sample	Sets 1–3	Ave.	Sample	Sets 1–3	Ave.
	12			13			18	
Baseline 1	18	11.7	Al_2O_3 1	17	14.3	CP Ti 1	16	17.3
	15			13			18	
	11			21			11	
Baseline 2	8	10.3	Al_2O_3 2	17	17	CP Ti 2	17	16
	12			13			20	
	13			11			19	
Baseline 3	5	8.7	Al_2O_3 3	13	12.3	CP Ti 3	17	17
	8			13			15	
	8			11			15	
Baseline 4	10	8.7	Al_2O_3 4	15	13	CP Ti 4	12	14.7
	8			13			17	
	9			11			17	
Baseline 5	7	8	Al_2O_3 5	16	14.7	CP Ti 5	16	17.3
	8			17			19	
	9			15			13	
Baseline 6	7	7.3	Al_2O_3 6	16	17	CP Ti 6	15	14.3
	6			20			15	
Overall Ave.		9.1			14.7			16.1

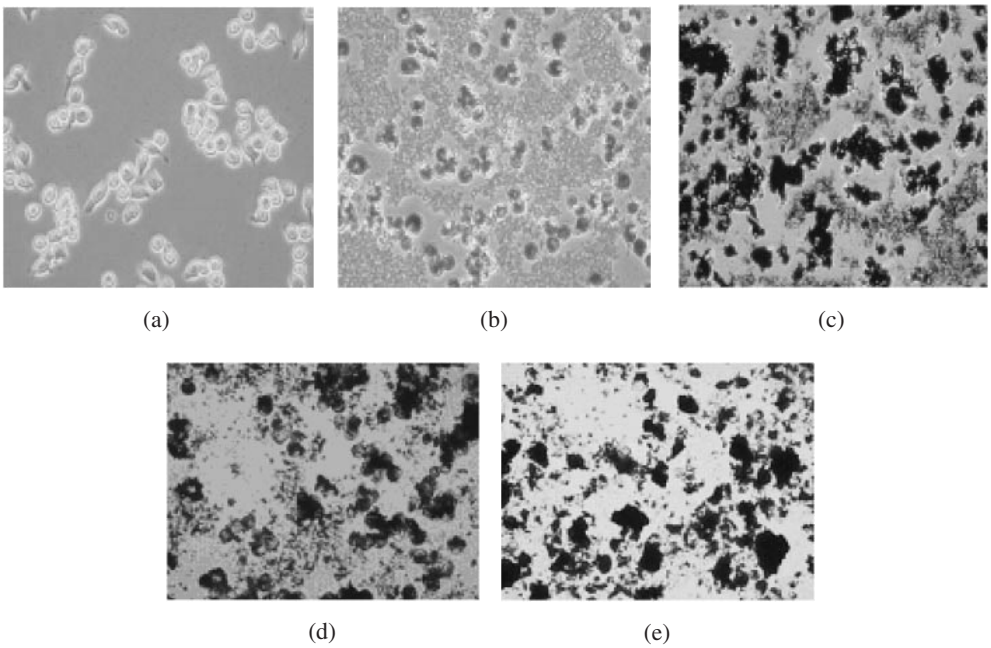

Fig. 8 OM images (40×) depicting particle phagocytosis of (a) control; (b) Al_2O_3; (c) CP Ti; (d) Ti–15Al–33Nb; and (e) Ti–21Al–29Nb by macrophages. All images were taken of stimulated cells after a 24-hour period of incubation in a 37°C incubator.

Al_2O_3- and CP Ti-treated samples was not statistically significant ($p = 0.07$). This agrees with the data from the methylene blue/acid fuchsin stain which showed bone deterioration is higher in Al_2O_3- and CP Ti-treated samples compared to baseline and Ti–Al–Nb alloy treated mice.

3.5 Immunohistochemistry

Qualitative analysis of the T-cells was performed by evaluating the immunohistochemistry stained samples for the amount of red color. Baseline, Al_2O_3, CP Ti, Ti–15Al–33Nb, and Ti–21Al–29Nb-treated calvaria slides were observed using the OM at 40× magnification, see Fig. 7. As the baseline samples had not been treated with the particles, one might expect a minimal number of T-cells in these samples. In agreement with theory the baseline slides exhibited few T-cells. The CP Ti treated calvaria showed intense reddish-brown staining indicating larger quantities of T-cells compared to baseline (as expected), while minimal staining was present in Ti–15Al–33Nb and Ti–21Al–29Nb-treated calvaria (similar to baseline samples). This indicates that the alloys induce less T-cell migration into calvarial tissues than the CP Ti. The least amount of T-cells was present in the Al_2O_3 samples which suggests that this material induces inflammation and bone erosion but not T cell infiltration.

3.6 Stimulation of Cells

OM images were taken of untreated as well as Al_2O_3-, CP Ti,- Ti–15Al–33Nb-, and Ti–21Al–29Nb-stimulated macrophages, see Fig. 8. All images were of stimulated cells after a 24-hour period of incubation in a 37°C incubator. After only 24 hours, the macrophages have engulfed nearly all of the particles in the vicinity of each cell as indicated by the density of particles in each cell and the clear zone containing no particles surrounding each individual macrophage or cluster of cells. In comparing the four different materials, all cells reacted nearly equally to the particles, and all macrophages consumed the particles with no apparent harm to the cell itself (cells are still viable).

Table 4 TNFα stimulation as a function of particle type.

Particle Type	Dose	Peak TNFα level (pg/mL)
none		12.8
CP Ti	10^7 particles/mL	1175
Alumina	0.001 M	42.8
Ti–15Al–33Nb	0.01 M	25.5
Ti–21Al–29Nb	0.01 M	25

3.7 TNFα Production

TNFα is a critical inflammatory cytokine involved in inducing inflammation and bone erosion. TNFα is produced when macrophages phagocytose particulate material, therefore, particles which stimulate more TNFα are likely to cause more inflammation and bone deterioration and indicate poor biocompatibility. Table 4 shows that CP Ti particles stimulate 100-fold more TNFα than untreated macrophages. The Al_2O_3 and both Ti–Al–Nb alloys induced slight increases in TNFα concentration compared to the untreated macrophages but significantly less than CP Ti particles ($p = 0.01$). These results agree with the animal studies, showing that the CP Ti particles are the most reactive and that the two different Ti–Al–Nb alloys exhibit similar behavior and show promise as potential implant materials.

4. Summary and Conclusions

The degree of biocompatibility of the novel Ti–Al–Nb alloys investigated were evaluated and compared to that for

CP Ti and Al_2O_3. Particle-treated calvaria underwent several tests to observe the deterioration of the bone, presence of osteoclasts, and T-cells. The various stains used were methylene blue/acid fuchsin, TRAcP, and immunohistochemistry. Overall, the Ti–Al–Nb alloys reacted favorably with mouse hard and soft tissue forming a solid coherent interface without significant cell swelling. The biocompatibility experiments involving measuring the resorption of mouse calvarial tissue in response to the Ti–Al–Nb particles, indicated that no significant detrimental reaction occurs between Ti–Al–Nb alloy particles and living cells. For the particle-treated calvaria, Ti–15Al–33Nb exhibited a midline sagittal suture area comparable to that of untreated mice, and such experiments demonstrated that there is only a small difference in the biological response for this alloy and Ti–21Al–29Nb. Both of these alloys were clearly superior to CP Ti and Al_2O_3 with respect to bone deterioration. In the other biocompatibility evaluations, the Ti–Al–Nb alloys exhibited behavior superior to that for CP Ti, thereby demonstrating their capability as feasible biomaterial substitutes for CP Ti. The results did not statistically indicate which of the two alloy compositions was more desirable from a biomedical implant point of view. Overall, it is apparent that Ti–Al–Nb alloys have potential for biomedical implant applications, and it is proposed that Ti–Al–Nb alloys will be of considerable future interest for biomedical applications.

The following conclusions were obtained from this work:

(1) The Ti–15Al–33Nb and Ti–21Al–29Nb particles adhered well to the mice calvaria without significant detrimental reaction as observed through OM, SEM, and EDS analysis.
(2) With respect to bone deterioration, the ranking for the particles in order from greatest-to-least bone deterioration exhibited was: Al_2O_3, CP Ti, Ti–21Al–29Nb, Ti–15Al–33Nb.
(3) The CP Ti particles exhibited a similar number of osteoclasts compared to the Al_2O_3 particles for TRAcP stained samples, both of which were greater than the baseline number of osteoclasts.
(4) CP Ti particle treatment resulted in the greatest infiltration of T-cells followed by the Ti–15Al–33Nb and Ti–21Al–29Nb alloys. Al_2O_3 particles demonstrated the least infiltration of T-cells.
(5) Macrophages phagocytosed the Ti–15Al–33Nb, Ti–21Al–29Nb, CP Ti, and Al_2O_3 particles equally readily with no apparent harm to the cell itself.
(6) The Ti–Al–Nb alloy particles stimulated significantly less TNFα than Al_2O_3 and CP Ti, where the CP Ti particles exhibited the worst response by stimulating 100-fold more TNFα than untreated macrophages.

Acknowledgement

This work was supported by the New York State Office of Science and Technology for Academic Research (NYSTAR) Grant No. C020080. The authors are grateful to Ms Katherine Sieg (Alfred University) and Mr. Christopher Cowen (Michigan State University) for their technical assistance.

REFERENCES

1) W. H. Harris: Clin Orthop (1995) 46–53.
2) A. D. Hanssen and J. A. Rand: J. Bone Jt. Surg. Am. **70** (1988) 491–499.
3) S. M. Horowitz and M. A. Purdon: Calcif. Tissue Int. **57** (1995) 301–305.
4) T. T. Glant and J. J. Jacobs: J. Orthop. Res. **12** (1994) 720–731.
5) J. Y. Wang, B. H. Wicklund, R. B. Gustilo and D. T. Tsukayama: Biomaterials **17** (1996) 2233–2240.
6) A. S. Shanbhag, J. J. Jacobs, J. Black, J. O. Galante and T. T. Glant: J. Orthop. Res. **13** (1995) 792–801.
7) T. A. Blaine, P. F. Pollice, R. N. Rosier, P. R. Reynolds, J. E. Puzas and R. J. O'Keffe: J. Bone Joint Surg. Am. **79** (1997) 1519–28.
8) S. H. Lee, F. R. Brennan, J. J. Jacobs, R. M. Urban, D. R. Ragasa and T. T. Glant: J. Orthop. Res. **15** (1997) 40–49.
9) A. A. Ragab, R. Van De Motter, S. A. Lavish, V. W. Goldberg, J. T. Ninomiya, C. R. Carlin and E. M. Greenfield: J. Orthop. Res. **17** (1999) 803–809.
10) S. R. Goldring, A. L. Shiller, M. S. Roelke, C. M. Rourke, D. A. O'Neil and W. H. Harris: J. Bone Joint Surg. Am. **65** (1983) 575–584.
11) S. R. Goldring, M. Jasty, M. S. Roelke, C. M. Rourke, F. R. Bringhurst and W. H. Harris: Arthritis. Rheum. **29** (1986) 836–842.
12) A. S. Shanbhag, J. J. Jacobs, J. Black, J. O. Galante and T. T. Glant: J. Arthroplasty **10** (1995) 498–506.
13) Y. Kadoya, P. A. Revell, N. al-Saffar, A. Kobayashi, G. Scott and M. A. Freeman: J. Orthop. Res. **14** (1996) 473–482.
14) D. R. Bertolini, G. E. Nedwin, T. S. Bringman, D. D. Smith and G. R. Mundy: Nature **319** (1986) 516–518.
15) C. S. Lader and A. M. Flanagan: Endocrinology **139** (1998) 3157–3164.
16) N. al-Saffar and P. A. Revell: Br J. Rheumatol **33** (1994) 309–316.
17) T. A. Blaine, R. N. Rosier, J. E. Puzas, R. J. Looney, P. R. Reynolds, S. D. Reynolds and R. J. O'Keefe: J. Bone Joint Surg. Am. **78** (1996) 1181–1192.
18) K. Kobayashi, N. Takahashi, E. Jimi, N. Udagawa, M. Takami, S. Kotake, N. Nakagawa, M. Kinosaki, K. Yamaguchi, N. Shima, H. Yasuda, T. Morinnaga, K. Higashio, T. J. Martin and T. Suda: J. Exp. Med. **191** (2000) 275–286.
19) E. M. Schwarz and R. J. O'Keefe: Arthritis Rheum. **41** (1998) S345.
20) K. D. Merkel, J. M. Erdmann, K. P. McHugh, Y. Abu-Amer, F. P. Ross and S. L. Teitelbaum: Am. J. Pathol **154** (1999) 203–210.
21) Y. H. Kim, J. S. Kim and S. H. Cho: J. Arthroplasty **14** (1999) 538–548.
22) D. Fender, W. M. Harper and P. J. Gregg: J. Bone Jt. Surg. Br. **81** (1999) 577–581.
23) J. J. Callaghan, E. E. Forest, J. P. Olejniczak, D. D. Goetz and R. C. Johnston: J. Bone Jt. Surg. Am. **80** (1998) 704–714.
24) G. C. McKay, R. Macnair, C. MacDonald and M. H. Grant: Biomaterials **17** (1996) 1339–1344.
25) ASTM designation F2066-01: Standard specification for wrought titanium-15 molybdenum alloy for surgical implant applications, (ASTM, Philadelphia. PA: U.S.A., 2001) 1605–1608.
26) ASTM designation draft #3. Standard specification for wrought taitanium-35Niobium-7zirconium-5tantalum alloy for surgical implant applications (UNS R58350): (ASTM, Philadephia. PA, U.S.A.).
27) M. Niinomi: Metall. Mater. Trans. **33A** (2002) 477–486.
28) M. F. Lopez, J. A. Jimenez and A. Gutierrez: Electrochimica Acta **48** (2003) 1395–1401.
29) M. Metikos-Hukovic, E. Tkalcec, A. Kwokal and J. Piljac: Surface and Coatings Technology **165** (2003) 40–50.
30) Z. Cai, T. Shafer, I. Watanabe, M. E. Nunn and T. Okabe: Biomaterials **24** (2003) 213–218.
31) D. Iijima, T. Yoneyama, H. Doi, H. Hamanaka and N. Kurosaki: Biomaterials **24** (2003) 1519–1524.
32) M. A. Khan, R. L. Williams and D. F. Williams: Biomaterials **20** (1999) 631–637.
33) M. Papakyriacou, H. Mayer, C. Pypen, H. Plenk Jr and S. Stanzl-Tschegg: International Journal of Fatigue **22** (2000) 873–888.
34) M. F. Semlitsch, H. Weber, R. M. Streicher and R. Schon: Biomaterials **13** (1992) 781–788.
35) I. Watanabe, Y. Tanaka, E. Watanabe and K. Hisatsune: The Journal of

Prosthetic Dentistry **92** (2004) 278–282.
36) T. Akahori, M. Niinomi, K. Fukunaga and I. Inagaki: Metall. Mater. Trans. **31A** (2000) 1949–1958.
37) C. J. Boehlert, C. J. Cowen, C. R. Jaeger, M. Niinomi and T. Akahori: Mater. Sci. Eng. C: Biomimetic and Supramolecular Systems **25** (2005) 263–275.
38) Henceforth these alloys will be referred to as Ti–15Al–33Nb and Ti–21Al–29Nb.
39) J. P. Krathovil: Light Scattering: Anal. Chem. **36** (1964) 458R.
40) M. Kerker: Scattering of Light and Other Electromagnetic Radiation (Academic Press, New York, 1969) 1.
41) E. M. Schwarz, E. B. Benz, A. P. Lu, J. J. Goater, A. V. Mollano, R. N. Rosier, J. E. Puzas and R. J. O'Keefe: Journal of Orthopedic Research **18** (2000) 849–855.
42) L. M. Childs, J. J. Goater, R. J. O'Keefe and E. M. Schwarz: Journal of Bone and Mineral Research **16** (2001) 338–347.
43) J. J. Goater, R. J. O'Keefe, R. N. Rosier, J. E. Puzas and E. M. Schwarz: Journal of Orthopedic Research **20** (2002) 169–173.
44) K. A. Rider and L. M. Flick: Analytical and Quantitative Cytology and Histology **26** (2004) 246–248.